



**HAL**  
open science

## **Dynamics of propagating front into sand ripples under regular waves**

Julie Lebunetel-Levaslot, Armelle Jarno-Druaux, Alexander Ezersky, François Marin

► **To cite this version:**

Julie Lebunetel-Levaslot, Armelle Jarno-Druaux, Alexander Ezersky, François Marin. Dynamics of propagating front into sand ripples under regular waves. *Physical Review E : Statistical, Nonlinear, and Soft Matter Physics* [2001-2015], 2010, 82 (3), <10.1103/PhysRevE.82.032301>. <hal-02095110>

**HAL Id: hal-02095110**

**<https://hal.science/hal-02095110v1>**

Submitted on 10 Apr 2019

**HAL** is a multi-disciplinary open access archive for the deposit and dissemination of scientific research documents, whether they are published or not. The documents may come from teaching and research institutions in France or abroad, or from public or private research centers.

L'archive ouverte pluridisciplinaire **HAL**, est destinée au dépôt et à la diffusion de documents scientifiques de niveau recherche, publiés ou non, émanant des établissements d'enseignement et de recherche français ou étrangers, des laboratoires publics ou privés.



HAL Authorization

# 1 Dynamics of propagating front into sand ripples under regular waves

2 J. Lebunetel-Levaslot,<sup>1</sup> A. Jarno-Druaux,<sup>1</sup> A. B. Ezersky,<sup>2</sup> and F. Marin<sup>1,\*</sup>

3 <sup>1</sup>Laboratoire Ondes et Milieux Complexes, FRE CNRS 3102, Université du Havre, 25 rue Philippe Lebon, BP 540,  
4 76058 Le Havre Cedex, France

5 <sup>2</sup>Laboratoire Morphodynamique Continentale et Côtière, UMR CNRS 6143, Université de Caen, 2-4 rue des Tilleuls,  
6 14000 Caen, France

7 (Received 9 April 2010; revised manuscript received 20 July 2010)

8 The results of an experimental study of pattern formation on sandy bottom under the action of regular  
9 harmonic surface waves are reported. It is found that two modes of pattern formation occur: sand ripples form  
10 uniformly on the whole bottom or from localized nucleation sites. In the second regime, the ripples appear in  
11 isolated regions (patches) increasing in size, and front propagation speed is measured. A simple dynamical  
12 model based on the Ginzburg-Landau equation is proposed to explain the characteristics of patches.

14 DOI: XXXX

PACS number(s): 45.70.Qj

## 15 I. INTRODUCTION

16 Pattern formation on a bottom under the action of surface  
17 waves has been investigated theoretically and experimentally  
18 for many years. The morphological characteristics of sand  
19 ripple patterns observed in the near shore region are impor-  
20 tant for the prediction of the dissipation of waves energy, and  
21 for the sediment transport. Ripples also influence the biological  
22 processes occurring on the bottom and the dispersion of  
23 pollutants. Ayrton [1] and Bagnold [2] carried out the pio-  
24 neering works on these structures. Detailed investigations of  
25 the onset of instability caused by oscillating water over sand  
26 were performed in [3,4]. The formation of vortices at the lee  
27 side of the ripple crest and their ejection upward at flow  
28 reversal were considered in [5,6]. These vortices control the  
29 mass transfer between neighboring ripples during their for-  
30 mation [6,7], and the wavelength of fully developed ripples  
31 is proportional to the amplitude of the oscillatory flow [6,8].  
32 The stability of bottom patterns in relation to changes of  
33 amplitude and frequency of water oscillations was studied in  
34 [9].

35 In this paper, we focus on the investigation of the ampli-  
36 fication of initial perturbations of small amplitude leading to  
37 the formation of sand ripples. The front propagation plays a  
38 key role in the involved processes, and we present in this  
39 brief report a detailed investigation of the characteristics of  
40 this front. The study of front propagation has been consid-  
41 ered in different unstable systems [10], and in particular in  
42 numerous hydrodynamic systems [11–13]. The phenomenon  
43 of front propagation for sand ripples under waves was men-  
44 tioned in [2]. However, this propagation has not been accu-  
45 rately investigated to our knowledge. The aim of the present  
46 paper is to study the features of front propagation in sand  
47 ripple patterns. The main difference between sand ripples  
48 and the systems considered in [11–13] is the following. The  
49 action of regular surface waves (propagating usually in one  
50 direction) results in anisotropy of the sand ripples instability,  
51 and consequently of the front propagation velocity, whereas  
52 the systems studied in [11–13] may be considered as isotro-  
53 pic. The characteristics of fronts propagating in the same

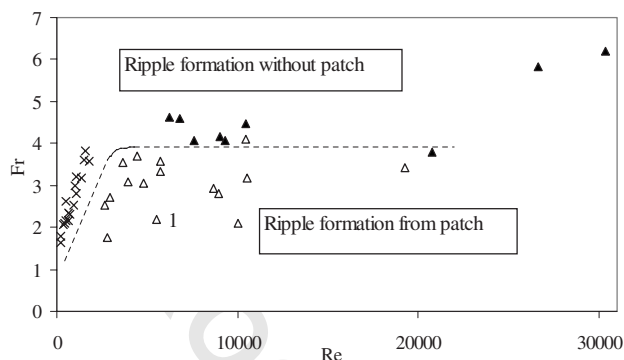
direction as surface waves or in the opposite direction are 54  
investigated in detail in the present study. 55

## 56 II. EXPERIMENTAL SETUP AND RESULTS

57 The experiments were performed in a 10 m long, 0.5 m  
58 high, and 0.49 m wide wave flume at Le Havre University.  
59 Regular surface waves were produced by an oscillating  
60 paddle at one end of the flume. At the other end a porous  
61 beach was installed to minimize wave reflection. The tempo-  
62 ral evolution of the free surface was measured with two fixed  
63 resistive probes and analyzed with Goda's method [14]. The  
64 reflection coefficient was less than 5% for all of the tests.  
65 The mean water depth at rest was  $d_* = 27$  cm. Experiments  
66 were carried out in a large range of wave and sediment  
67 parameters:  $0.95 \text{ s} \leq T \leq 2.2 \text{ s}$ ,  $0.045 \text{ m} \leq H \leq 0.099 \text{ m}$ ,  
68  $111 \mu\text{m} \leq d_{50} \leq 375 \mu\text{m}$ , where  $T$  and  $H$  are the wave pe-  
69 riod and height, respectively, and  $d_{50}$  the median grain size.  
70 For each test, the bed was initially flat and covered by a 25  
71 mm sand layer. In spite of the care taken to flatten the bot-  
72 tom, some defects of flatness are observed. The maximum  
73 amplitude of perturbations is approximately 2 mm. The bed  
74 deformation was measured from the first excitation cycles  
75 with an optical method, detailed in [15]. The spatial reso-  
76 lution in the horizontal and vertical directions was 0.5 mm/  
77 pixel. The dimensions of the processed field were 5.46 m  
78 long and 0.325 m width. The ripples wavelengths at the equi-  
79 librium state were in the range  $28.4 \text{ mm} \leq \lambda \leq 77 \text{ mm}$  for  
80 present tests. Characteristics of ripples were obtained using  
81 the one-dimensional (1D) -Hilbert transform. A great advan-  
82 tage of this technique is that in each patch the amplitude and  
83 phase of ripples may be determined.

84 Two distinct modes of ripple patterns formation are ob-  
85 served. In the first mode, any perturbation on the bottom is  
86 enough to trigger ripple formation and ripples form uni-  
87 formly on the whole bed. In the second mode, patterns form  
88 from isolated rippled zones (described as patches by Faraci  
89 and Foti [16]). For present tests, patches appeared in zones  
90 where the characteristic amplitude of disturbances was  
91 greater or equal to the critical value of 2 mm. Two nondi-  
92 mensional parameters were used to characterize the regime  
93 of pattern formation: the Reynolds number  $Re$  and the  
94 Froude number  $Fr$ . These parameters are defined as follows:

\*Corresponding author. francois.marin@univ-lehavre.fr



× Jarno-Druaux et al., 2004    △ Present tests, patch    ▲ Present tests, without patch

FIG. 1. Delineation of the two observed modes of ripple formation in the (Re,Fr) plane, indicating the boundary (dashed line) between the modes with and without patch (the test for which Re = 5512 and Fr = 2.2 is identified with the label 1).

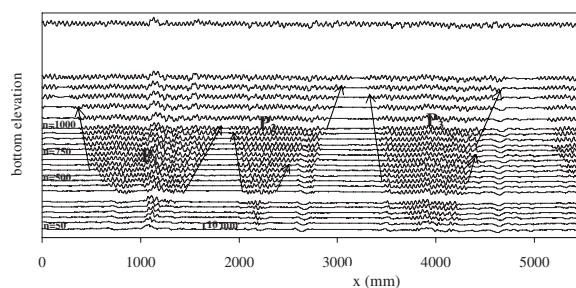


FIG. 3. Bottom elevation as a function of the  $x$ -longitudinal position and number of excitation cycles (Re=5512, Fr=2.2). The arrows show the ripple front positions detected for the three patches P1, P2, and P3.

95  $Re = U_\infty b / \nu$ ,  $Fr = U_\infty / \sqrt{(s-1)gd_{50}}$ , where  $b$  and  $U_\infty$  are the  
 96 fluid particle semicircursion and the fluid velocity amplitude  
 97 at the edge of the bed boundary layer, respectively,  $s$  is the  
 98 relative density of sediment,  $g$  the acceleration due to grav-  
 99 ity, and  $\nu$  the water kinematic viscosity. The delineation of  
 100 the two observed modes of ripple formation in the (Re,Fr)  
 101 plane is presented in Fig. 1. The data of Jarno-Druaux *et al.*  
 102 [17] obtained in the same wave flume with lightweight grains  
 103 of relative density 1.35 and median grain diameter  $170 \mu\text{m}$   
 104 are also shown in this figure. Present tests show that for fixed  
 105 values of Re, there is a critical value  $Fr_{cr}$  of the Froude  
 106 number below which ripples form from localized sites; for  
 107  $Fr > Fr_{cr}$ , no “patch” is observed. The critical Froude number  
 108 becomes independent of the Reynolds number for Re  
 109  $> 5000$ . This suggests that for  $Fr_{cr} = Fr_{cr,max} \approx 3.9$ , the sedi-  
 110 ments move all over the bottom with a very low resistance to  
 111 motion for every hydrodynamic conditions and ripples can  
 112 form everywhere on the bottom. When  $Fr < Fr_{cr,max}$ , the in-  
 113 ertial effects become more important for increasing values of  
 114 Re (keeping constant the value of Fr), and the bed local  
 115 perturbations lead to patches formation. The critical value  
 116  $Fr_{cr}$  grows with Re when  $Fr < Fr_{cr,max}$ . This may result from  
 117 a decrease of the gravity effects in comparison with the in-  
 118 ertial effects acting on the grains for increasing values of Fr  
 119 for a given value of Re ( $< 5000$ ), leading to a higher mobil-  
 120 ity of the grains and preventing patch formation.

121 In order to study the front propagation, we focus on a test  
 122 for which a slow dynamics of pattern formation from ampli-  
 123 tude defects is observed. We have Re=5512 and Fr=2.2 for  
 124 this test, and the mean ripple wavelength is  $\lambda = 42 \text{ mm}$  at the  
 125 equilibrium state. An example of bed image in gray levels is  
 126 given in Fig. 2 for  $n = 800$  excitation cycles where three main  
 127 patches are clearly identified (P1 to P3). The temporal evo-  
 128 lution of the bottom elevation is plotted as a function of the

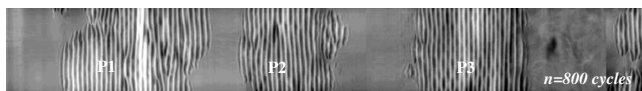


FIG. 2. Example of bed image in gray levels for  $n = 800$  cycles (Re=5512, Fr=2.2). P1 to P3 refer to the three processed patches.

$x$ -longitudinal position in Fig. 3, for  $y = 0.20 \text{ m}$  where the  $y$  129  
 axis refers to the cross-section direction. The origin of the  $x$  130  
 axis is situated at 2.3 m from the wave paddle, increasing 131  
 values of  $x$  corresponding to shorter distances from the ab- 132  
 sorbing beach. The time step is equal to 50 cycles for the first 133  
 1000 cycles, and afterward to 100 cycles. Isolated systems of 134  
 propagating ripples can be observed during more than 1000 135  
 cycles before the invasion of the whole bottom. The estima- 136  
 tion of front velocities can then be performed on a long time 137  
 for the three observed patches. The bottom elevation signal 138  
 $\eta(x,t)$  of each patch is cut into two parts in order to process 139  
 the two fronts separately. The Fourier spectra of signals are 140  
 then calculated and harmonics are filtered. After this filtering 141  
 process, we get  $\eta(x,t) = \eta_m(x,t)\cos[kx + \varphi(x,t)]$ , where 142  
 $\eta_m(x,t)$  is for the slow varying amplitude,  $\varphi(x,t)$  is the slow 143  
 varying phase of the bottom profile, and  $k$  is the bottom wave 144  
 number. 145

Using the Hilbert transform, 146

$$\hat{\eta}(x,t) = \frac{1}{\pi} PV \left[ \int_{-\infty}^{+\infty} \frac{\eta(x,t)}{x-\chi} d\chi \right] = \eta_m(x,t) \sin[kx + \varphi(x,t)] \quad (1) \quad 147$$

where  $PV$  denotes principal value, it is possible to determine 148  
 the phase and amplitude of sand ripples on the flume bottom 149  
 and compare with the theoretical predictions. We can consid- 150  
 er the bottom profile as the real part of a complex function 151  
 $\eta(x,t) = \text{Re}\{A(x,t)\exp[i(kx)]\}$  with  $A(x,t) = |A(x,t)|e^{i\varphi(x,t)}$  and 152  
 where 153

$$|A(x,t)| = a = \sqrt{\eta^2(x,t) + \hat{\eta}^2(x,t)}, \quad \varphi(x,t) = \arctan\left(\frac{\hat{\eta}}{\eta}\right) - kx. \quad (2) \quad 154$$

We extract the module of the complex amplitude  $a$  and the 155  
 phase  $\varphi(x,t)$  from the signals. An example of the spatial 156  
 dependence for  $a(x)$  and  $\varphi(x)$  is shown in Fig. 4. It is impor- 157  
 tant to emphasize that large changes of phase occur at wave 158  
 front. The wave front is localized in the region where a tran- 159  
 sition from a low amplitude to a high (nearly constant) value 160  
 is detected. We have chosen the following criterion to deter- 161  
 mine the front position: the front is situated in the region 162  
 where the value of the amplitude is equal to 15% of the 163  
 maximum value for the patch. The ripple fronts are presented 164  
 in Fig. 3. They propagate linearly with time, and a good 165  
 coefficient of regression (in the range 0.70–0.98) is obtained. 166  
 The up-flow ( $v_{p-}$ ; propagation in the direction opposite to the 167

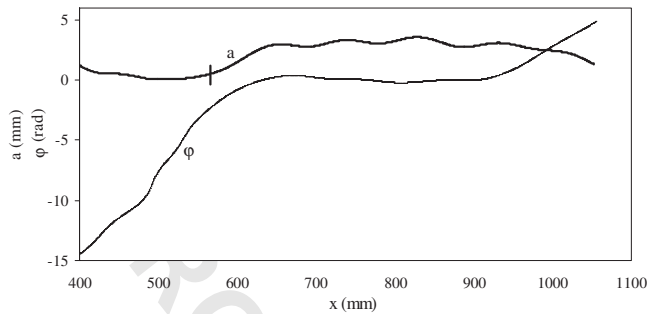


FIG. 4. Example of spatial distribution for the amplitude (bold line) and phase (thin line) of sand ripples for a front propagating upward (Patch P1,  $t=550$  wave excitation cycles). The segment crossing the bold line delineates the border between the flat bottom and the ripple patch according to the criterion of threshold amplitude.

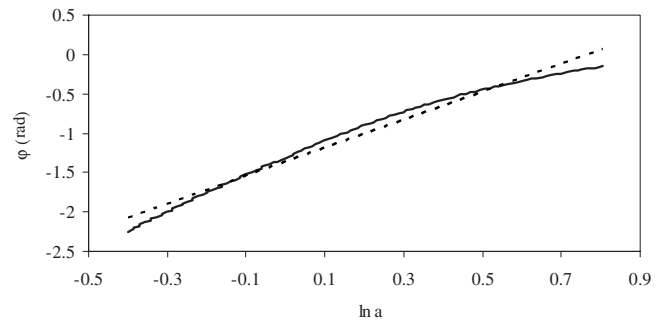


FIG. 5. Dependence of the wave phase  $\varphi$  on the logarithm of wave amplitude  $\ln a$  for  $462 \text{ mm} < x < 520 \text{ mm}$  (bold curve) with its best linear fit approximation ( $\varphi=1.82 \ln a - 1.52$ ; square of the correlation coefficient  $R^2=0.96$ ; dashed line);  $t=700$  wave excitation cycles.

168 surface waves propagation) and down-flow ( $v_{p+}$ ; propagation  
169 in the same direction as the surface waves) front velocities of  
170 the patches are given in Table I. The results show that the  
171 fronts propagating in the direction of surface wave propaga-  
172 tion have greater velocities than the fronts propagating in the  
173 opposite direction ( $|v_{p+}| > |v_{p-}|$ ).

### 174 III. DISCUSSION OF RESULTS

175 According to the present experimental results, the front  
176 propagation may be considered as an envelope wave, and we  
177 have found the amplitude and phase of this envelope. Let us  
178 compare the experimental results with the solution of an  
179 equation describing the envelope amplitude, the complex  
180 Ginzburg-Landau equation (GLE) which is widely used to  
181 investigate pattern dynamics [18]. Present experiments show  
182 us that there is a threshold value of the initial bed perturba-  
183 tions in the front propagation regime: perturbations with an  
184 amplitude less than a critical value decay with time, whereas  
185 perturbations with an amplitude greater than the critical  
186 value grow. To take this effect into account, it is necessary to  
187 keep the nonlinear terms proportional to the third and fifth  
188 degrees of amplitude in the GLE (quintic version of GLE)  
189 [10]. The cubic version of the GLE is able to describe the  
190 linear instability of infinitely small perturbations and the  
191 nonlinear amplitude saturation. The simplest model to de-  
192 scribe the front propagation in our system is the following:

$$193 \frac{\partial A}{\partial t} = (1 + ic_1) \frac{\partial^2 A}{\partial x^2} + \varepsilon A + (1 + ic_3)|A|^2 A - (1 - ic_5)|A|^4 A, \quad (3)$$

194 where  $A$  is the complex amplitude of sand ripples,  $\varepsilon$  the  
195 super criticality ( $\varepsilon < 0$  in our case), and  $c_1, c_3, c_5$  are real

TABLE I. Up-flow and down-flow patch velocities for the three patches P1, P2, and P3 ( $\text{Re}=5512$ ,  $\text{Fr}=2.2$ ).

Patch	Up-flow patch velocity $v_{p-}$ (mm s <sup>-1</sup> )	Down-flow patch velocity $v_{p+}$ (mm s <sup>-1</sup> )
1	-0.23	0.62
2	-0.19	0.64(400 < n < 650); 0.43(1000 < n < 1400)
3	-0.16	0.37(500 < n < 800); 0.52(900 < n < 1400)

coefficients for dispersion ( $c_1$ ), cubic nonlinearity ( $c_3$ ), and  
quintic nonlinearity ( $c_5$ ). The analytical solution of Eq. (3)  
has the following form [19]:  $A = e^{-i\Omega t} a(\xi) e^{i\phi(\xi)}$ ,  $\xi = x \mp Vt$   
where  $V$  is the front velocity and  $\Omega$  the frequency of sand  
ripples. The amplitude and phase obey the following differ-  
ential equations (ansatz):  $\partial a / \partial \xi = K_{L\mp} a (1 - a^2(\xi) / a_N^2)$ ,  
 $\partial \phi / \partial \xi = q_L + (q_N - q_L) a^2(\xi) / a_N^2$ . For propagating fronts, the  
solution has the following form:

$$a = a_N e^{K_{L\mp} \xi / \sqrt{1 + e^{2K_{L\mp} \xi}}}, \quad (4)$$

The amplitude grows exponentially from an infinitely  
small value to a constant value  $a_N$ . The six constants  $K_{L\mp}$ ,  $q_L$ ,  
 $q_N$ ,  $\Omega$ ,  $V$ ,  $a_N$  are determined by inserting the ansatz into  
Eq. (3) [10]. The sign “+” corresponds to a front which  
propagates in the positive direction (direction of surface  
waves propagation),  $K_{L+} < 0$ ,  $a(x=-\infty, t=0) = a_N$ ,  $a(x$   
 $= +\infty, t=0) = 0$ , and the sign “-” corresponds to a front  
propagating in the opposite direction:  $K_{L-} > 0$ ,  $a(x=-\infty, t$   
 $= 0) = 0$ ,  $a(x=+\infty, t=0) = a_N$ . It should be noted that for re-  
gions where  $a = a_N$ , we have  $\phi = q_N(x \mp Vt)$ , and for  $a \ll a_N$ ,  
 $\phi \approx q_L(x \mp Vt)$ . The profile of the sandy bottom may be  
written as  $\eta(x, t) = \text{Re}[A(x, t) \exp(ikx)] = a(x \mp Vt) \cos(\Omega t$   
 $- q_{N,L}(x \mp Vt) - kx)$ . This means that  $q_L$  and  $q_N$  may be con-  
sidered as infinitesimal and finite amplitude additional terms  
for the wave number of sand ripples, respectively. Using the  
 $a_N^2$  expression from the first equation of ansatz, we find a  
correlation between the phase and amplitude derivatives:  
 $\partial \phi / \partial \xi = q_N - [(q_N - q_L) \partial a / \partial \xi] / a K_{L\pm}$ , and after integration we  
get

$$\phi = q_N \xi - [(q_N - q_L) / K_{L\mp}] \ln a. \quad (5)$$

Excluding a linear growth of the phase with space for a given  
instant, we are able to present a local correlation between the  
wave amplitude  $a(x)$  and the wave phase  $\varphi(x)$ :  $\varphi(x) = (q_L$   
 $- q_N) \ln a / K_{L\pm}$ . Such correlation really occurs for the wave  
front in sand ripples. Figure 5 shows an example of the  
variation of the phase  $\varphi$  with the amplitude  $a$ . Using the best  
linear fit approximation (dashed line in Fig. 5), we deter-  
mined the coefficient  $\kappa_{\pm} = (q_L - q_N) / K_{L\pm}$ . The results are dif-  
ferent for the fronts propagating in the direction of surface  
waves and in the opposite direction. The values of the coef-  
ficient  $\kappa_{\pm}$  are estimated for both fronts of Patch 1, for dif-  
ferent numbers of excitation cycles; these values are given in

237 Table II. It can be noted that the linear dependence between  
 238 the phase  $\varphi$  and  $\ln a$  is obtained with lower values of the  
 239 regression coefficient for fronts propagating in the direction  
 240 of surface waves (except when  $t=950$  excitation cycles). In  
 241 this case, for some instants, no estimation of  $\kappa_+$  could be  
 242 proposed. The fronts propagating in the direction of surface  
 243 waves are then not as regular as the fronts propagating in the  
 244 opposite direction. We were able to estimate the coefficient  
 245  $K_{L\pm}$ : the solution (4) shows us that this exponent may ap-  
 246 proximate the amplitude growth on the wave front. Using an  
 247 exponential approximation of experimental data, we have  
 248 found different coefficients for the fronts: the averaged value  
 249 for  $K_{L+}$  was  $K_{L+} = -0.047 \text{ mm}^{-1}$ , and for the front propagat-  
 250 ing in the opposite direction,  $K_{L-} = 0.03 \text{ mm}^{-1}$ . The front  
 251 propagating in the direction of surface waves is “steeper”  
 252 than the front propagating in the opposite direction. We have  
 253 estimated the changes in wave number due to the finite am-  
 254 plitude of sand ripples:  $q_L - q_N \approx 0.039 \text{ mm}^{-1}$  for waves co-  
 255 directed with the surface waves, and  $q_L - q_N \approx 0.025 \text{ mm}^{-1}$   
 256 for waves propagating in the opposite direction. In both  
 257 cases, the finite amplitude leads to a decrease in wave num-  
 258 ber  $k + q_N$  in comparison with the linear wave number  $k + q_L$ ,  
 259 but this effect is larger for the front propagating in the direc-  
 260 tion of surface waves.

261 The differences between the characteristics of the fronts  
 262 propagating in the same direction as the surface waves and in  
 263 the opposite direction may be due to the drift induced by  
 264 surface waves. It is well known [20] that in the bed boundary  
 265 layer above a flat bed, induced flows lead to mass transport  
 266 in the direction of waves propagation. Above sand ripples,  
 267 the momentum transfer and suspended sediment dynamics  
 268 are dominated by the formation and shedding at flow reversal  
 269 of lee wake vortices [21]. Present data involve weakly asym-  
 270 metrical waves ( $B < 0.1$  where  $B = 3bk_{sw}/4 \sinh^2(k_{sw}d_*)$  and  
 271  $k_{sw}$  is the surface wave number). Using a one-dimensional  
 272 vertical (1DV) two-layer model where vortex shedding is  
 273 represented in the lower layer by a time-varying eddy vis-  
 274 cosity, Davies and Thorne [21] have shown that the near-bed  
 275 sand transport is in the direction of surface waves propaga-  
 276 tion for weakly asymmetrical waves. Such transport of sand  
 277 increases the front velocity  $v_{p+}$  and decreases the velocity

278  $v_{p-}$ .  
 303  
 304  
 305

306 [1] H. Ayrton, *Proc. R. Soc. London, Ser. A* **84**, 285 (1910).  
 307 [2] R. A. Bagnold, *Proc. R. Soc. London, Ser. A* **187**, 1 (1946).  
 308 [3] P. Blondeaux, *J. Fluid Mech.* **218**, 1 (1990).  
 309 [4] E. Foti and P. Blondeaux, *Coastal Eng.* **25**, 227 (1995).  
 310 [5] V. Marieu *et al.*, *J. Geophys. Res.* **113**, C09007 (2008).  
 311 [6] K. H. Andersen *et al.*, *Phys. Rev. E* **63**, 066308 (2001).  
 312 [7] E. K. O. Hellén and J. Krug, *Phys. Rev. E* **66**, 011304 (2002).  
 313 [8] T. Schnipper *et al.*, *Phys. Rev. E* **78**, 047301 (2008).  
 314 [9] J. L. Hansen *et al.*, *Nature (London)* **410**, 324 (2001).  
 315 [10] W. van Saarloos, *Phys. Rep.* **386**, 29 (2003).  
 316 [11] J. Fineberg and V. Steinberg, *Phys. Rev. Lett.* **58**, 1332 (1987).  
 317 [12] J. Fineberg *et al.*, *Phys. Rev. A* **41**, 5743 (1990).  
 318 [13] M. Fermigier *et al.*, *J. Fluid Mech.* **236**, 349 (1992).

TABLE II. Values of the inclination coefficient for the upstream and downstream fronts and different numbers of excitation cycles (Patch P1). The linear regression coefficients are given in parentheses.

Number of excitation cycles	$\kappa_- = \frac{q_L - q_N}{K_{L-}}$	$\kappa_+ = \frac{q_L - q_N}{K_{L+}}$
550	+1.30(R <sup>2</sup> =0.99)	
600	+0.33(R <sup>2</sup> =0.99)	
650	+0.45(R <sup>2</sup> =0.99)	-1.20(R <sup>2</sup> =0.95)
700	+1.80(R <sup>2</sup> =0.97)	
750	+0.66(R <sup>2</sup> =0.99)	-0.12(R <sup>2</sup> =0.75)
800	+1.80(R <sup>2</sup> =0.99)	-0.49(R <sup>2</sup> =0.81)
850	+0.60(R <sup>2</sup> =0.99)	-0.51(R <sup>2</sup> =0.85)
900	+0.31(R <sup>2</sup> =0.94)	-2.30(R <sup>2</sup> =0.93)
950	+0.28(R <sup>2</sup> =0.87)	-0.33(R <sup>2</sup> =0.98)

IV. CONCLUSIONS

We have shown that depending on the values of the control parameters (Froude and Reynolds numbers), sand ripples on the bottom may arise as a result of two types of bifurcation: spatially homogeneous growth of small perturbations, and appearance of patches. In the last case, wave front propagation occurs. Using the Hilbert transform, we measured the amplitude and phase of ripple waves, and we have found coincidences between the experimental characteristics of propagating fronts and the analytical solution of van Saarloos and Hohenberg [19]. Such coincidences allowed us to find a correlation between the sand ripples amplitude and wave number, and conclude that there exists an effect of wave number decrease due to the finite amplitude of sand ripples. Our measurements agree with the measurements of other researchers (see, for example, [16]): the spatial period of sand ripples increases with increasing ripples amplitude. We have found that the propagating front characteristics depend on the direction of surface waves which generate ripples. If the front propagates in the direction of surface waves, it has a larger celerity, is steeper and more irregular than the front which propagates in the opposite direction. In our opinion such differences are caused by the mean flow induced by surface waves near the bottom.

[14] Y. Goda, *Random Seas and Design of Marine Structures* (World Scientific, Singapore, 2000).  
 [15] F. Marin and A. B. Ezersky, *Eur. J. Mech. B/Fluids* **27**, 251 (2008).  
 [16] C. Faraci and E. Foti, *Phys. Fluids* **13**, 1624 (2001).  
 [17] A. Jarno-Druaux *et al.*, *Eur. J. Mech. B/Fluids* **23**, 695 (2004).  
 [18] I. S. Aranson and L. Kramer, *Rev. Mod. Phys.* **74**, 99 (2002).  
 [19] W. van Saarloos and P. C. Hohenberg, *Phys. Rev. Lett.* **64**, 749 (1990).  
 [20] M. S. Longuet-Higgins, *Philos. Trans. R. Soc. London, Ser. A* **245**, 535 (1953).  
 [21] A. G. Davies and P. D. Thorne, *J. Geophys. Res.* **110**, C05017 (2005).